Article

Corrosion Inhibition Properties of Phenyl Phthalimide Derivatives against Carbon Steel in the Acidic Medium: DFT, MP2, and Monte Carlo Simulation Studies

Saprizal Hadisaputra,* Agus Abhi Purwoko, Aliefman Hakim, Niko Prasetyo, and Saprini Hamdiani

Read Online

ACCESS		Metrics & More		Article Recommendations

ABSTRACT: The effectiveness of phenyl phthalimide and its derivatives at preventing corrosion of carbon steel has been tested experimentally using gravimetric and electrochemical measurements. However, experimental studies have not thoroughly explained the structural patterns and coating mechanisms of phenyl phthalimide and its derivatives during corrosion inhibition. In this study, the density functional theory (DFT), ab initio MP2, and Monte Carlo simulation are applied to study phenyl phthalimide (PP) and its derivatives as corrosion inhibitors of carbon steel. The geometry, quantum parameters, and reactive site of the inhibitors were determined by DFT and ab initio MP2 methods. The real environment conditions of corrosion inhibition in the solution phase can be replicated by the Monte Carlo simulation. The corrosion inhibition efficiency of phthalimide derivatives is $PP\text{-}OCH_3 > PP\text{-}CH_3 > PP\text{-}H > PP\text{-}Cl > PP\text{-}NO_2$. The theoretical study is consistent with previously reported experimental results.
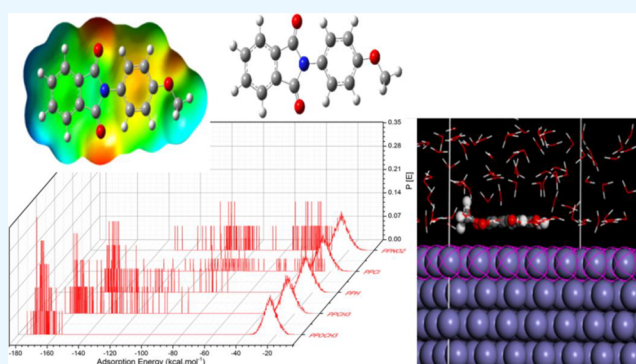
1. INTRODUCTION

Carbon steel has been widely used in various applications, such as structural components, industrial pipes, and kitchen utensils.[1] Carbon steel is highly susceptible to corrosion in the oil and gas industry.[2] Corrosion of carbon steel in the environment can harm the economy.[3] Therefore, corrosion inhibition in carbon steel is desirable because of its excellent mechanical properties and low cost but feeble corrosion resistance.[4,5] Corrosion inhibition is often used with the addition of an inhibitor.[6] Inhibitors are one of the most efficient ways to prevent corrosion from attacking carbon steel.[7−9] A suitable inhibitor requires heteroatoms like sulfur, nitrogen, and oxygen and π-bonds that can be used to form complexes with metals.[10−12] Organic inhibitors have high corrosion inhibition efficiency values and are environmentally friendly.[13−15]

Phenyl phthalimide is an aromatic organic compound that has oxygen and nitrogen heteroatoms. These atoms act as electron donors in the corrosion inhibition process. Experimental studies have previously reported the corrosion inhibition of phthalimide derivatives on copper in nitric acid using weightloss and polarization techniques. The highest inhibition efficiency value was obtained for the N-(3-methoxyphenylaminomethyl) phthalimide at 67.8%.[16] Zaafarany tested the corrosion inhibition of phenyl phthalimide and its derivatives on carbon steel in sulfuric acid media using weightloss and polarization techniques. The highest inhibition efficiency value with the addition of an OCH_3 substituent was obtained at 92.36%. An OCH_3 substituent acts as an electron donor so that the adsorption is stronger, increasing the value of the inhibition efficiency.[17]

Experimental studies have accurately determined the efficiency of corrosion inhibition, but the detailed explanation of why OCH_3 contributes the most to corrosion inhibition has not been explained in detail. Research time and costs are high. The theoretical study, which is now supported by adequate software and hardware, becomes a bridge for these problems. The corrosion inhibition efficiency depends on the molecule's electron density, which can be calculated with high accuracy by theoretical studies. Theoretical studies are as critical as experimental ones in testing corrosion inhibition in a molecule. The use of quantum chemical calculations can predict the adsorption site during the corrosion inhibition process.[18,19] Quantum chemical calculations can provide answers to questions about experimental findings based on the inter-
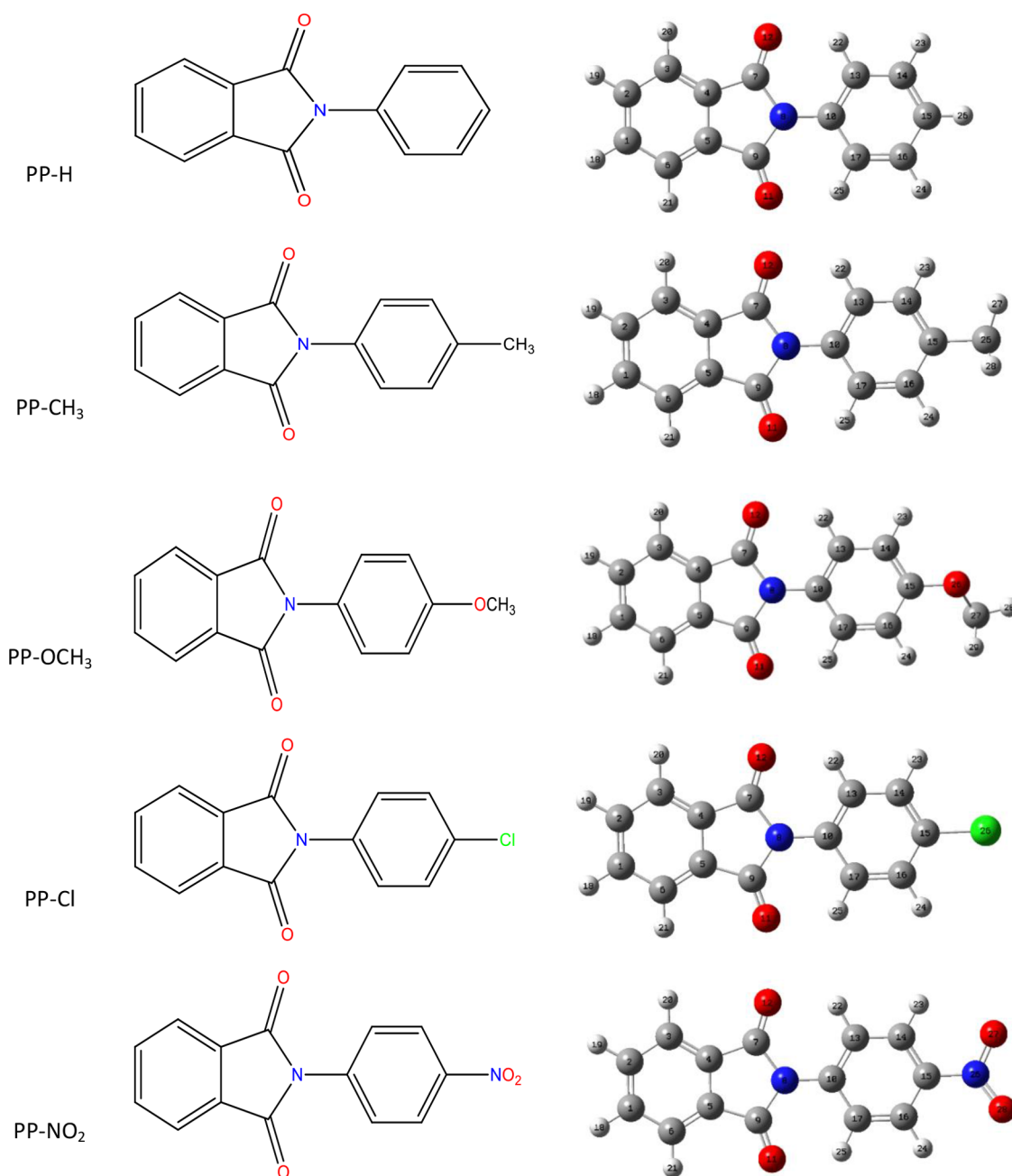
Figure 1. 2D and 3D structure of PP-H, PP-CH$_3$, PP-OCH$_3$, PP-Cl, and PP-NO$_2$.

actions of organic inhibitors with metal surfaces.[20,21] The approaches of density functional theory,[22,23] ab initio,[24,25] and molecular dynamic simulation[26−28] can provide a thorough explanation of each inhibitor's performance in relation to its orientation and structure, as well as the process by which an inhibitor adheres to metal surfaces. Hadisaputra et al. used density functional theory (DFT) at different theoretical levels, ab initio, and Monte Carlo simulation to predict caffeine and hydrocoumarin derivatives' copper corrosion inhibition performance.[29,30] Donor- and electron-withdrawing groups, as well as the orientation of the molecule, all affect how strongly organic corrosion inhibitors interact with the surface of metals.[31−33] In this study, the effects of quantum parameters and the molecule's adsorption process on the corrosion inhibition of phenyl phthalimide derivatives on metal surfaces are tested.

2. METHODS

2.1. Quantum Chemical Calculations. Calculations based on quantum chemistry were used to predict the molecular geometry, electron distribution, and transfer from corrosion inhibitors. Figure 1 depicts the structure of a targeted inhibitor molecule. The molecular geometry calculation is accelerated by first optimizing the geometry using the DFT method B3LYP/6-31G(d). DFT and ab initio MP2 methods at 6-311++G (d,p) were used to re-optimize the structures of 4PP-H, PP-CH$_3$, PP-OCH$_3$, PP-Cl, and PP-NO$_2$ in the gas phase. The influence of solvents is incorporated into the computation using a polarized continuum model built on the Gaussian code. The dielectric constant of water is 78.4. For solvent phase energetics, single-point computations of gas-phase geometries are sufficient. Previous research found that it had a minor impact on structure and energy.[34−36] The
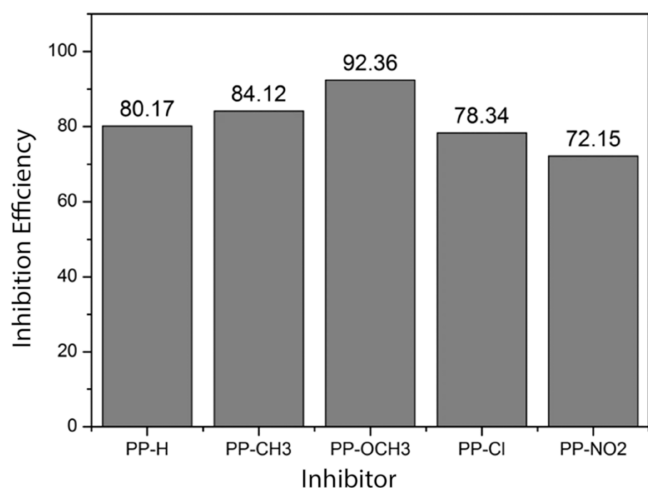
Figure 2. Inhibitory efficiency of phenyl phthalimide and its derivatives in the KI synergic effect environment.

Table 1. Crystal Structures of Phenyl Phthalimide Derivatives Experimentally[50] and DFT/6-311++G (d,p)

bond length (Å)	exp[50]	theory	bond angle (°)	exp[50]	theory
N1−C1	1.4089	1.42832	C1−N1−C9	124.34	125.25679
N1−C2	1.4148	1.42832	C2−N1−C9	123.42	125.25679
N1−C9	1.4214	1.43919	N1−C9−C10	119.38	120.51544
C1−O1	1.2093	1.21393	N1−C9−C14	119.11	120.51544
C2−O2	1.2053	1.21393			

Gaussian 09 program calculates all quantum chemical and geometric parameters.[37]

Based on DFT and ab initio methods, quantum chemistry characteristics including electron affinity (A), electronegativity (χ), hardness (η), energy of highest occupied molecular orbitals (EHOMO) and energy of lowest unoccupied molecular orbitals (ELUMO), gab energy (E), ionization potential (I), and the number of electron transfers (N) were computed. The ionization potential (I) and electron affinity (A) are correlated with the HOMO and LUMO energy values in each organic inhibitor.[38]

$$I = -\text{EHOMO} \tag{1}$$

$$A = -\text{ELUMO} \tag{2}$$

The electronegativity (χ) and hardness (η) of the inhibitor can be determined using eqs 3 and 4.[39]

$$\chi = \frac{(I + A)}{2} \tag{3}$$

$$\eta = \frac{(I - A)}{2} \tag{4}$$

Equation 5 can be used to determine the number of electrons transferred (N) from the inhibitor to the metal.[40]

$$\Delta N = \frac{\chi\text{Fe} - \chi\text{Inh}}{2(\eta\text{Fe} + \eta\text{Inh})} \tag{5}$$

where χ^{Fe} and χ^{Inh} are the absolute electronegativity values of Fe and organic inhibitors. η^{Fe} and η^{Inh} are the absolute hardness values of Fe and organic inhibitors, respectively. The number of electrons transferred was calculated using theoretical values of $\chi^{\text{Fe}} = 7.00$ eV and $\eta^{\text{Fe}} = 0$ eV.[41,42]

Equations 6 and 7 can be used to calculate the Fukui index to determine nucleophilic (f_K^+) and electrophilic (f_K^-) attacks.[43]

$$f_K^+ = q_k(N+1) - q_k(N) \tag{6}$$

$$f_K^- = q_k(N) - q_k(N-1) \tag{7}$$

In organic inhibitors, $q_k(N+1)$ is the atomic charge ($+1$), $q_k(N)$ is the atomic charge (neutral), and $q_k(N-1)$ is the atomic charge (-1).[43]

2.2. Monte Carlo Simulation. Material Studio 7.0 from Accelrys Inc. was used to perform the Monte Carlo simulation.[44,45] Monte Carlo simulation was used to help find the inhibitor's reactive site for adsorption at the lowest energy on the metal surface.[46] The following weight percentages apply to the carbon steel type (L-52): 0.26% C, 1.35% Mn, 0.04% P, 0.05% S, 0.05% Nb, 0.02% V, 0.03% Ti, and 98.2% Fe.[7] Thus, the Fe(110) plane can represent the surface of carbon steel. The Fe(110) crystal plane was the most

Table 2. Phenyl Phthalimide and Its Derivatives' Quantum Chemical Properties with B3LYP/6-311++G(d,p) and MP2/6-311++G(d,p) in Gaseous Media

inhibitors	EHOMO eV	ELUMO eV	ΔE eV	I eV	A eV	χ eV	η eV	ΔN eV
PP-H								
B3LYP	−6.5914	−2.7639	−3.8276	6.5914	2.7639	4.6776	1.9138	0.6067
MP2	−8.6094	0.8376	−9.4470	8.6094	−0.8376	3.8859	4.7235	0.3296
PP-CH₃								
B3LYP	−6.3558	−2.7149	−3.6409	6.3558	2.7149	4.5353	1.8204	0.6769
MP2	−8.3313	0.8506	−9.1819	8.3313	−0.8506	3.7403	4.5910	0.3550
PP-OCH₃								
B3LYP	−5.9944	−2.6942	−3.3002	5.9944	2.6942	4.3443	1.6501	0.8047
MP2	−8.0815	0.8514	−8.9330	8.0815	−0.8514	3.6150	4.4665	0.3789
PP-NO₂								
B3LYP	−7.3286	−3.1783	−4.1503	7.3286	3.1783	5.2534	2.0751	0.4208
MP2	−9.5292	0.5157	−10.0448	9.5292	−0.5157	4.5068	5.0224	0.2482
PP-Cl								
B3LYP	−6.5933	−2.9051	−3.6882	6.5933	2.9051	4.7492	1.8441	0.6103
MP2	−8.7033	0.7714	−9.4747	8.7033	−0.7714	3.9659	4.7374	0.3202

Table 3. Phenyl Phthalimide and Its Derivatives' Quantum Chemical Properties with B3LYP/6-311++G(d,p) and MP2/6-311++G(d,p) in Aqueous Media

inhibitors	EHOMO eV	ELUMO eV	ΔE eV	I eV	A eV	χ eV	η eV	ΔN eV
PP-H								
B3LYP	−6.7280	−2.7658	−3.9623	6.7280	2.7658	4.7469	1.9811	0.5686
MP2	−8.8149	0.9723	−9.7871	8.81498.800[59]	−0.9723	3.9213	4.8936	0.3146
PP-CH₃								
B3LYP	−6.5030	−2.7484	−3.7546	6.5030	2.7484	4.6257	1.8773	0.6324
MP2	−8.5487	0.9848	−9.5335	8.5487	−0.9848	3.7820	4.7668	0.3375
PP-OCH₃								
B3LYP	−6.1745	−2.7426	−3.4319	6.1745	2.7426	4.4586	1.7160	0.7405
MP2	−8.3408	0.9837	−9.3245	8.3408	−0.9837	3.6786	4.6623	0.3562
PP-NO₂								
B3LYP	−7.2176	−3.1538	−4.0638	7.2176	3.1538	5.1857	2.0319	0.4465
MP2	−9.4252	0.6063	−10.0315	9.4252	−0.6063	4.4095	5.0157	0.2582
PP-Cl								
B3LYP	−6.6880	−2.8044	−3.8836	6.6880	2.8044	4.7462	1.9418	0.5803
MP2	−8.8494	0.9344	−9.7839	8.8494	−0.9344	3.9575	4.8919	0.3110

Table 4. Phenyl Phthalimide and Its Derivatives' Quantum Chemical Properties with B3LYP/6-311++G(d,p) and MP2/6-311++G(d,p) in Gaseous Media

inhibitors	EHOMO eV	ELUMO eV	ΔE eV	I eV	A eV	χ eV	η eV	ΔN eV
protonated PP-H								
B3LYP	−10.9199	−7.4010	−3.5190	10.9199	7.4010	9.1604	1.7595	−0.6139
MP2	−13.0125	−3.5331	−9.4794	13.0125	3.5331	8.2728	4.7397	−0.1343
protonated PP-CH₃								
B3LYP	−10.6095	−7.3171	−3.2923	10.6095	7.3171	8.9633	1.6462	−0.5963
MP2	−12.7953	−3.4613	−9.3341	12.7953	3.4613	8.1283	4.6670	−0.1209
protonated PP-OCH₃								
B3LYP	−9.9401	−7.2872	−2.6528	9.9401	7.2872	8.6136	1.3264	−0.6083
MP2	−12.4008	−3.4648	−8.9360	12.4008	3.4648	7.9328	4.4680	−0.1044
protonated PP-NO₂								
B3LYP	−11.1833	−7.7283	−3.4550	11.1833	7.7283	9.4558	1.7275	−0.7108
MP2	−13.8008	−3.9040	−9.8968	13.8008	3.9040	8.8524	4.9484	−0.1872
protonated PP-Cl								
B3LYP	−10.5950	−7.4924	−3.1026	10.5950	7.4924	9.0437	1.5513	−0.6587
MP2	−13.0299	−3.6548	−9.3751	13.0299	3.6548	8.3423	4.6876	−0.1432

Table 5. Phenyl Phthalimide and Its Derivatives' Quantum Chemical Properties with B3LYP/6-311++G(d,p) and MP2/6-311++G(d,p) in Aqueous Media

inhibitors	EHOMO eV	ELUMO eV	ΔE eV	I eV	A eV	χ eV	η eV	ΔN eV
protonated PP-H								
B3LYP	−7.8353	−3.9304	−3.9048	7.8353	3.9304	5.8828	1.9524	0.2861
MP2	−9.9466	−0.0501	−9.8965	9.9466	0.0501	4.9983	4.9483	0.2023
protonated PP-CH₃								
B3LYP	−7.5974	−3.9138	−3.6836	7.5974	3.9138	5.7556	1.8418	0.3378
MP2	−9.7860	−0.0365	−9.7496	9.7860	0.0365	4.9112	4.8748	0.2142
protonated PP-OCH₃								
B3LYP	−7.0771	−3.9116	−3.1655	7.0771	3.9116	5.4944	1.5828	0.4756
MP2	−9.5085	−0.0414	−9.4671	9.5085	0.0414	4.7749	4.7336	0.2350
protonated PP-NO₂								
B3LYP	−8.3667	−4.0273	−4.3394	8.3667	4.0273	6.1970	2.1697	0.1851
MP2	−10.4846	−0.1521	−10.3324	10.4846	0.1521	5.3183	5.1662	0.1628
protonated PP-Cl								
B3LYP	−7.7131	−3.9663	−3.7467	7.7131	3.9663	5.8397	1.8734	0.3097
MP2	−10.0690	−0.0909	−9.9781	10.0690	0.0909	5.0800	4.9891	0.1924

stable for simulating the adsorption process.[47] Supercells were used (8 × 8) to provide a large surface for interacting with organic inhibitors. These simulations were carried out in a grid (19.859002 × 19.859002 × 34.187956) with periodic boundary conditions and a representative interface portion to be simulated without arbitrary boundary effects. The Fe(110) plane is used to build a vacuum slab with a thickness of 20 along the C axis. To optimize the structure of every system
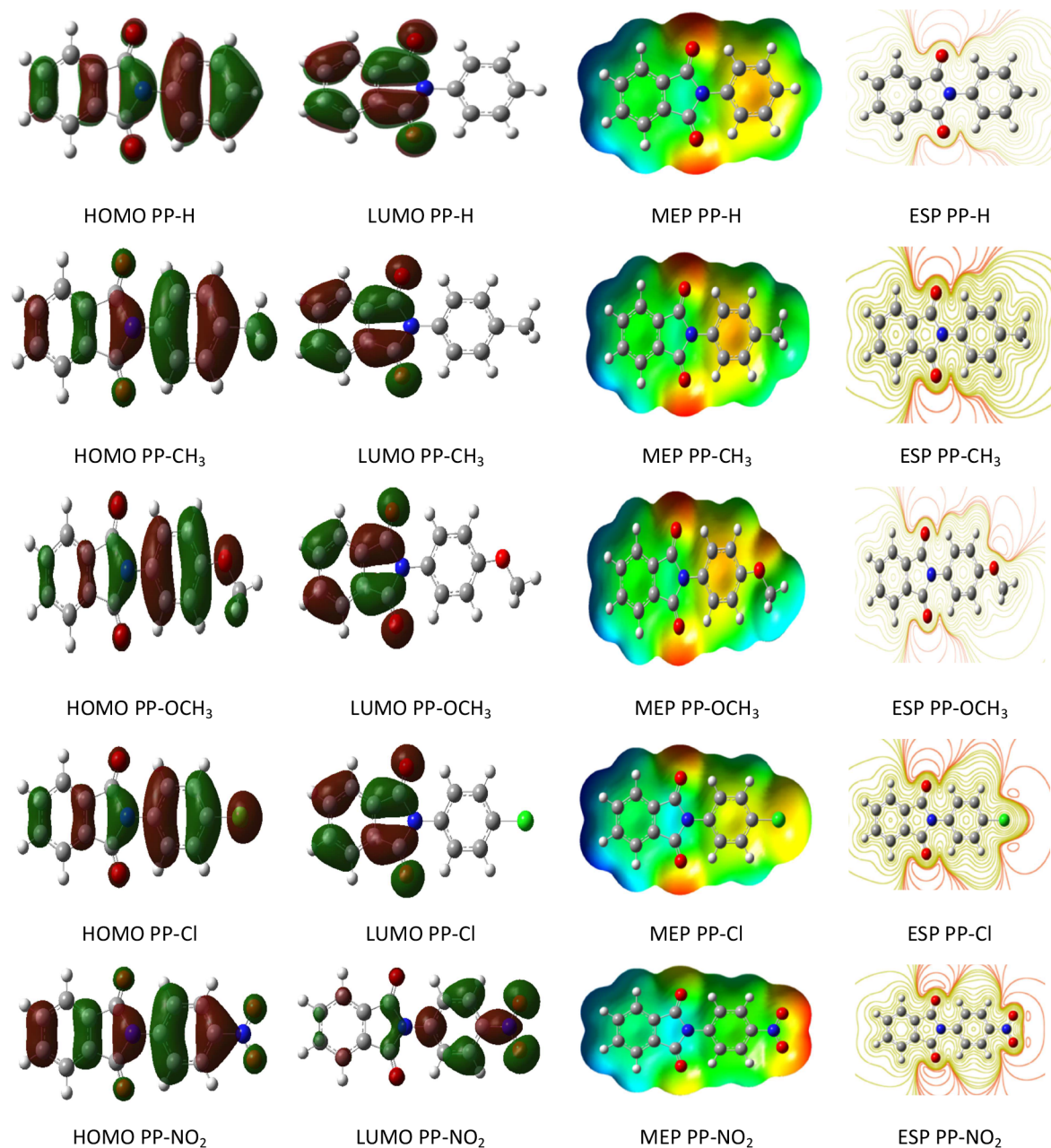
Figure 3. HOMO, LUMO, MEP, and ESP orbitals of PP-H, PP-CH$_3$, PP-OCH$_3$, PP-Cl, and PP-NO$_2$.

component under study, the COMPASS force field is used in all simulations.[30] Phenyl phthalimide derivatives (PP-H, PP-CH$_3$, PP-OCH$_3$, PP-Cl, and PP-NO$_2$) and Fe(110) with 100 water molecules were used. Water molecules are essential in the simulation to imitate the conditions of the corrosion process in the environment.[48,49]

3. RESULTS AND DISCUSSION

3.1. Quantum Chemical Parameters. Phenyl phthalimide and its derivatives as a corrosion inhibitor against carbon steels in sulfuric acid media have been reported previously.[17] Figure 2 depicts phenyl phthalimide's corrosion inhibition efficiency values and its derivatives in the KI synergic effect environment. Experimental studies show that OCH$_3$ provides the maximum contribution to the corrosion inhibition performance of phthalimide derivatives. Theoretical studies can complement experimental studies by explaining why

OCH$_3$ contributes significantly. The electronic properties and the reactive site of the inhibitor and the adsorption mechanism of the inhibitor on the metal surface can be explained theoretically.

Due to the selection of DFT and ab initio, method validation is carried out first to test the need for the method and basis set according to the system under study. The method and basis set at the DFT and MP2 levels 6-111++G (d,p) show the agreement between the experimental[50] and theoretical geometric parameters. Table 1 shows that the difference in the bond length is 0.0128, and the bond angle is 1.3236°. The difference is low, so the method and basis set can be used to calculate quantum chemical parameters and Fukui functions in the studied system.

Energy parameters provide important information about the electronic properties and reactivity of the corrosion inhibitors studied. The EHOMO value is associated with the electron-
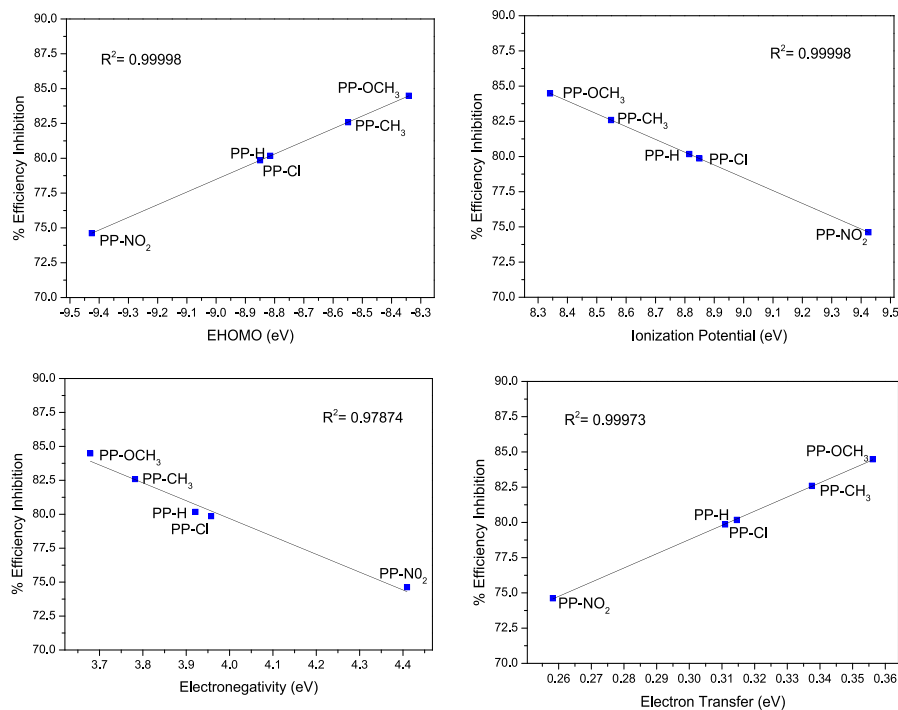
Figure 4. Correlation between the effectiveness of inhibition and quantum chemical properties of phenyl phthalimide and its derivatives, including electronegativity, ionization potential, and electron transfer in the gas phase.
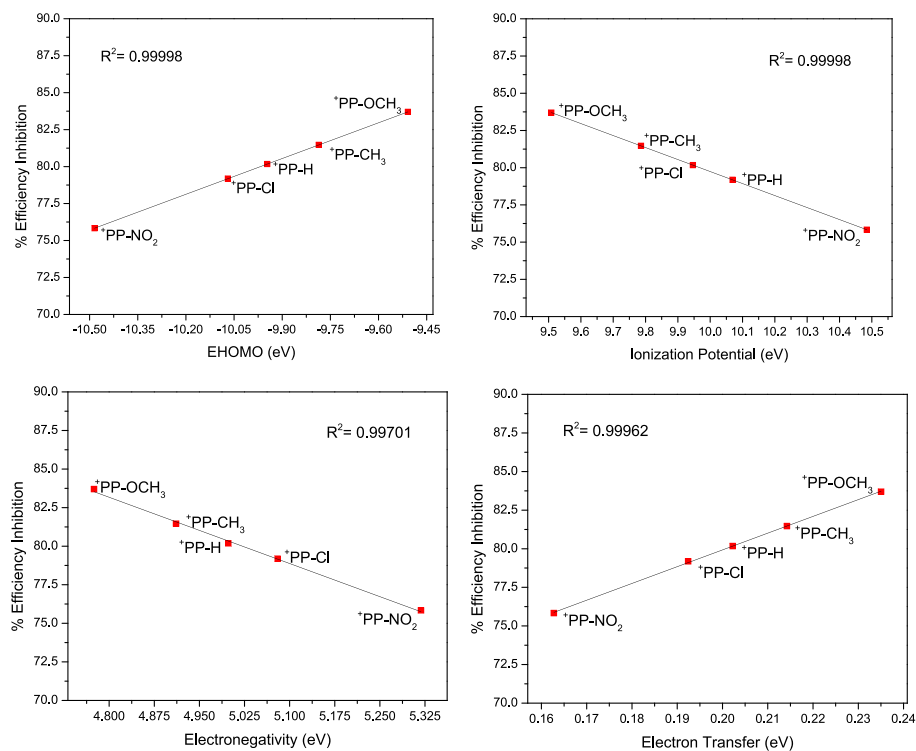

Figure 5. Correlation between the effectiveness of inhibition and quantum chemical properties of phenyl phthalimide and its derivatives, including electronegativity, ionization potential, and electron transfer under protonated conditions.

donating ability of the corrosion inhibitor. A high EHOMO value indicates that it is easier to donate electrons to empty d orbitals in metals. A high EHOMO value facilitates good adsorption to increase the value of corrosion inhibition efficiency by influencing the electron transport process through the adsorbed layer.[51,52] The EHOMO values obtained using

the DFT and ab initio MP2 methods are displayed in Tables 2345. PP-OCH$_3$ has the highest E$_{HOMO}$ value, -8.3408 eV (ab initio MP2). The order of E_{HOMO} values is PP-OCH$_3$ > PP-CH$_3$ > PP-H > PP-Cl > PP-NO$_2$. This explains that PP-OCH$_3$ can adhere more strongly than other inhibitors to the carbon steel surface. PP-OCH$_3$ has a lone pair of electrons that acts as

Table 6. Functional Analysis of PP-H, PP-CH$_3$, PP-OCH$_3$, PP-NO$_2$, and PP-Cl

PP-H	$q_k (N-1)$	$q_k N$	$q_k (N+1)$	f_K^+	f_K^-	PP-OCH$_3$	$q_k (N-1)$	$q_k N$	$q_k (N+1)$	f_K^+	f_K^-
C1	−0.3744	−0.331	−0.3135	0.0175	0.0435	C12	−0.3825	−0.3734	−0.3394	0.0340	0.0091
C2	−0.3744	−0.331	−0.3135	0.0175	0.0435	C13	−0.7113	−0.7092	−0.7493	−0.0401	0.0021
C3	−0.3700	−0.3314	−0.3387	−0.0073	0.0386	C14	0.0427	0.0615	0.1712	**0.1097**	0.0188
C4	0.1598	0.1933	0.2231	0.0298	0.0335	C15	0.1531	0.1861	0.2843	0.0982	0.0330
C5	0.1598	0.1933	0.2231	0.0298	0.0335	O16	−0.4709	−0.3107	−0.2628	0.0479	**0.1602**
C6	−0.3700	−0.3314	−0.3387	−0.0073	0.0386	O17	−0.4769	−0.3171	−0.2694	0.0477	**0.1598**
C7	0.1021	0.1815	0.1802	−0.0013	0.0794	O26	−0.2083	−0.1993	−0.0626	**0.1367**	0.0090
N8	0.0310	0.0827	0.1919	**0.1092**	0.0517	C27	−0.3359	−0.3397	−0.3762	−0.0366	−0.0038
C9	0.1021	0.1815	0.1802	−0.0013	0.0794	**PP-NO$_2$**	$q_k (N-1)$	$q_k N$	$q_k (N+1)$	f_K^+	f_K^-
C10	0.3984	0.3569	0.4130	0.0561	−0.0415	C1	−0.3202	−0.3154	−0.2868	0.0285	0.0048
C11	−0.0856	−0.0679	0.0011	0.0690	0.0177	C2	−0.3202	−0.3154	−0.2868	0.0285	0.0048
C12	−0.3225	−0.3072	−0.2736	0.0337	0.0153	C3	−0.3649	−0.3638	−0.3731	−0.0094	0.0011
C13	−0.402	−0.3843	−0.2669	**0.1174**	0.0177	C4	0.1015	0.1067	0.1401	0.0334	0.0052
C14	−0.3225	−0.3072	−0.2736	0.0337	0.0153	C5	0.1015	0.1067	0.1401	0.0334	0.0052
C15	−0.0856	−0.0679	0.0011	0.0690	0.0177	C6	−0.3649	−0.3638	−0.3731	−0.0094	0.0011
O16	−0.4713	−0.3116	−0.2521	0.0595	**0.1596**	C7	0.363	0.3731	0.3865	0.0134	0.0101
O17	−0.4713	−0.3116	−0.2521	0.0595	**0.1596**	N8	0.0784	0.1006	0.2248	**0.1242**	0.0222
PP-CH$_3$	$q_k (N-1)$	$q_k N$	$q_k (N+1)$	f_K^+	f_K^-	C9	0.363	0.3731	0.3865	0.0134	0.0101
C1	−0.3726	−0.328	−0.3138	0.0143	0.0446	C10	0.134	0.1776	0.207	0.0293	0.0437
C2	−0.3743	−0.3298	−0.3154	0.0144	0.0445	C11	−0.0002	0.0691	0.1591	0.0900	0.0693
C3	−0.3695	−0.3308	−0.338	−0.0072	0.0387	C12	−0.3903	−0.2964	−0.2455	0.0509	0.0939
C4	0.122	0.1451	0.1656	0.0205	0.0230	C13	−0.313	−0.4928	−0.5432	−0.0504	−0.1797
C5	0.1437	0.1676	0.1874	0.0199	0.0239	C14	−0.3903	−0.2964	−0.2455	0.0509	0.0939
C6	−0.3734	−0.335	−0.3421	−0.0071	0.0384	C15	−0.0002	0.0691	0.1591	**0.0900**	0.0693
C7	0.18	0.2659	0.2767	0.0108	0.0859	O16	−0.3195	−0.2945	−0.235	0.0596	0.0250
N8	0.0418	0.0933	0.1902	**0.0969**	0.0515	O17	−0.3195	−0.2945	−0.235	0.0596	0.0250
C9	0.1849	0.2701	0.2799	0.0098	0.0852	N18	−0.2314	−0.1622	−0.1303	0.0319	0.0692
C10	0.217	0.1778	0.2399	0.0621	−0.0391	O19	−0.2945	−0.051	−0.0026	0.0484	**0.2435**
C11	−0.2696	−0.2534	−0.2062	0.0472	0.0161	O20	−0.2945	−0.051	−0.0026	0.0484	**0.2435**
C12	−0.7164	−0.7098	−0.7218	−0.0120	0.0066	**PP-Cl**	$q_k (N-1)$	$q_k N$	$q_k (N+1)$	f_K^+	f_K^-
C13	0.2569	0.2712	0.3804	**0.1092**	0.0143	C1	−0.4238	−0.325	−0.3094	0.0155	0.0989
C14	−0.1904	−0.1681	−0.0863	0.0818	0.0223	C2	−0.4238	−0.325	−0.3094	0.0155	0.0989
C15	−0.0442	−0.0222	0.0447	0.0669	0.0220	C3	−0.5717	−0.323	−0.3293	−0.0063	**0.2487**
O16	−0.4697	−0.3095	−0.2539	0.0557	**0.1602**	C4	0.1696	0.0906	0.1097	0.0191	−0.0790
O17	−0.4766	−0.3167	−0.2612	0.0554	**0.1599**	C5	0.1696	0.0906	0.1097	0.0191	−0.0790
C18	−0.4911	−0.4903	−0.4869	0.0034	0.0008	C6	−0.5717	−0.323	−0.3293	−0.0063	**0.2487**
PP-OCH$_3$	$q_k (N-1)$	$q_k N$	$q_k (N+1)$	f_K^+	f_K^-	C7	0.1409	0.2952	0.3029	0.0077	0.1543
C1	−0.3717	−0.3272	−0.3164	0.0108	0.0445	N8	0.0526	0.0934	0.1899	**0.0965**	0.0408
C2	−0.3748	−0.3317	−0.3218	0.0099	0.0432	C9	0.1409	0.2952	0.3029	0.0077	0.1543
C3	−0.3892	−0.3499	−0.3555	−0.0056	0.0392	C10	−0.0926	−0.1077	−0.0605	0.0473	−0.0151
C4	0.1012	0.1142	0.1276	0.0135	0.0130	C11	−0.286	−0.266	−0.2121	0.0539	0.0201
C5	0.2003	0.2358	0.2542	0.0184	0.0355	C12	−0.5387	−0.4433	−0.4001	0.0432	0.0955
C6	−0.3418	−0.3000	−0.3053	−0.0054	0.0419	C13	0.165	0.3493	0.3732	0.0239	0.1843
C7	0.0557	0.1334	0.1368	0.0034	0.0777	C14	−0.5388	−0.4433	−0.4001	0.0432	0.0955
N8	0.0428	0.0865	0.1780	**0.0920**	0.0519	C15	−0.286	−0.266	−0.2121	0.0539	0.0201
C9	0.2588	0.3508	0.3614	0.0106	0.0920	O16	−0.4627	−0.3089	−0.255	0.0539	0.1538
C10	0.1786	0.1438	0.2311	0.0873	−0.0348	O17	−0.4627	−0.3089	−0.255	0.0539	0.1538
C11	−0.0843	−0.0735	−0.0311	0.0424	0.0108	Cl18	0.4442	0.4379	0.6654	**0.2275**	−0.0063

an electron-donating group so that it can transfer more electrons to the carbon steel surface to form complex compounds.

Therefore, the theoretical study concluded the same as the experimental study that PP-OCH$_3$ contributed maximally to the corrosion inhibition efficiency. In contrast, a low ELUMO value indicates that the inhibitor prefers to accept electrons from the metal.[53,54] Tables 2−5 show the lowest ELUMO value for PP-NO$_2$ at 0.6063 eV. PP-NO$_2$ is more likely to be electron-withdrawing and accepts more electrons from carbon steel than other inhibitors, so it is not strongly adsorbed on the

carbon steel surface. Figure 3 depicts the electron distribution in molecular orbitals of PP-OCH$_3$, PP-CH$_3$, PP-H, PP-Cl, and PP-NO$_2$. The difference in electron distribution between the three compounds is noticeable, with PP-OCH$_3$ having a more extensive electron distribution. This improves inhibitor performance by strengthening the predicted E_{HOMO}-related sequence.

The value of the ionization potential is directly related to E_{HOMO}.[55] The ionization potential value is the least amount of energy needed for electrons to attach to the surface of the metal and shield it from the corrosive medium. As a result, the
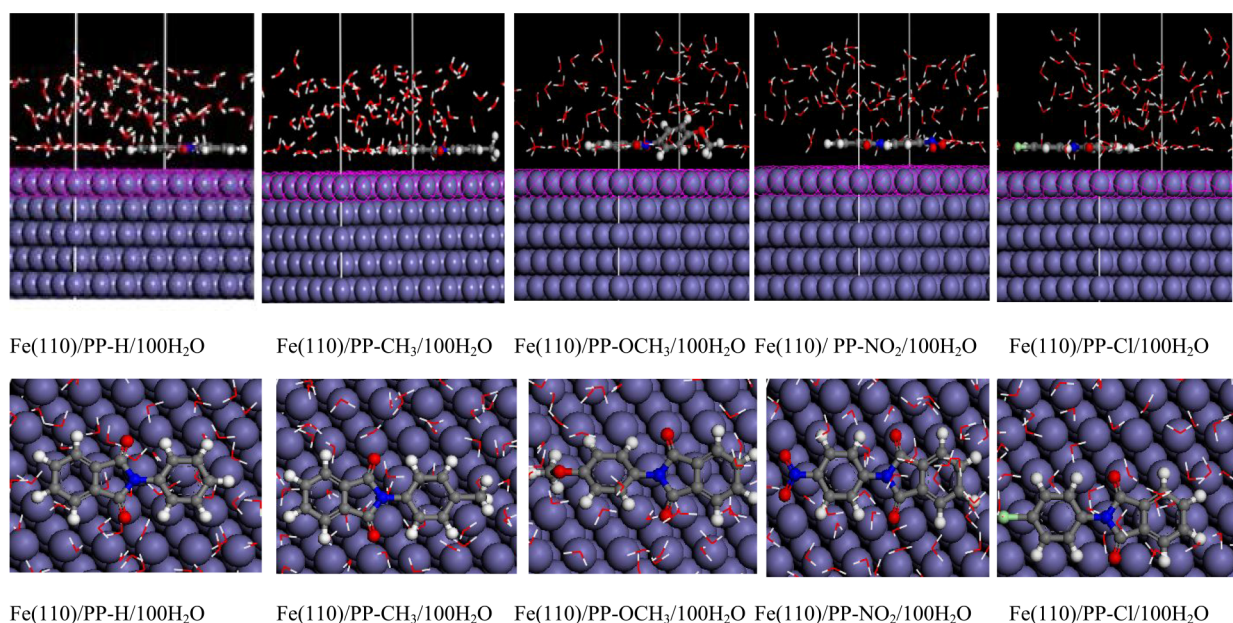
Figure 6. Adsorption of phenyl phthalimide and its derivatives on the surface of ferrous metals in the Monte Carlo Fe(110)/inhibitor/100H$_2$O system.

Table 7. Energy of Phenyl Phthalimide Adsorption and Fe(110)/Inhibitor/100H$_2$O System Derivatives Based on Monte Carlo Simulation

systems	energy adsorption (inhibitor) kcal mol^{-1}	adsorption energy (water) kcal mol^{-1}
neutral inhibitor		
Fe(110)/PP-H/100H$_2$O	−150.40607559	−13.26304026
Fe(110)/PP-CH$_3$/100H$_2$O	−162.60596435	−12.28170340
Fe(110)/PP-OCH$_3$/100H$_2$O	−173.59120922	−11.90185293
Fe(110)/PP-Cl/100H$_2$O	−138.72615845	−12.81391923
Fe(110)/PP-NO$_2$/100H$_2$O	−130.48848970	−12.81391923
protonated inhibitor		
Fe(110)/PP-H/100H$_2$O	−157.30443499	−12.09552923
Fe(110)/PP-CH$_3$/100H$_2$O	−167.05417030	−10.65878790
Fe(110)/PP-OCH$_3$/100H$_2$O	−172.29703093	−14.46829434
Fe(110)/PP-Cl/100H$_2$O	−148.12364859	−14.62546890
Fe(110)/PP-NO$_2$/100H$_2$O	−129.66083150	−15.48199690

low ionization potential (I) indicates the ease with which the atom can release its outer electron. It can donate electrons to the metal surface, thus increasing corrosion inhibition efficiency.[56,57] Equation 1 can be used to calculate the ionization potential value. Table 3 shows the quantum chemical parameters of phenyl phthalimide and its derivatives in aqueous media. Table 3 shows that PP-OCH$_3$ has the lowest ionization potential value (8.3408 eV) compared to PP-CH$_3$, PP-H, PP-Cl, and PP-NO$_2$, the values of which are 8.5487, 8.8149, 8.8494, and 9.4252 eV, respectively. In comparison to PP-CH$_3$, PP-H, PP-Cl, and PP-NO$_2$, PP-OCH$_3$ is anticipated

to have a better inhibitory efficiency value. This also explains why PP-NO$_2$ has the lowest corrosion inhibition efficiency, with the lowest 9.4252 eV. This ionization potential value can also be used to validate the theoretical calculation methods. The DFT ionization potential value is far below the standard experimental value.[58] Experimentally, the PP-H ionization potential is 8.80 eV,[59] whereas DFT/6-311++G(d,p) yields a value of 6.7280 eV. DFT/potential B3LYP's ionization value is 2 eV lower than the experimental results. This demonstrates DFT's weakness in imitating the energy of experimental results. We therefore advise against using DFT to determine the energy of a molecule's quantum parameter.

High electronegativity values indicate that organic corrosion inhibitors are electron acceptors, while low ones indicate corrosion inhibitors as electron donors. This is because corrosion inhibitors with low electronegativity values will be easier to donate electrons or more reactive.[60−62] Electronegativity values can be calculated using eq 3. Tables 2−5 depict that the order of electronegativity values is PP-OCH$_3$ < PP-CH$_3$ < PP-Cl < PP-H < PP-NO$_2$. PP-OCH$_3$ has the lowest electronegativity value of 3.6786 eV calculated by MP2/6-311++G(d,p). The electronegativity of PP-OCH$_3$ is lower than that of iron, 7 eV. PP-OCH$_3$ will donate its electrons to carbon steel. Therefore, PP-OCH$_3$ acts as the most effective corrosion inhibitor than other inhibitors. The theoretical value of electronegativity has a linear correlation with the efficiency of corrosion inhibition (Figures 4 and 5).

A high electron transfer value, according to Koopmans, enhances the value of corrosion inhibition efficiency.[38] Tables 2−5 show the fraction of electrons, and the electron transfer values can be calculated using eq 5. Table 3 shows the N of the inhibitors using the MP2/6-311++G (d,p) method. The highest electron transfer value in PP-OCH$_3$ is 0.3562 eV. The order of electron transfer values is PP-OCH$_3$ > PP-CH$_3$ > PP-H > PP-Cl > PP-NO$_2$. This electron transfer value is consistent with the previously published corrosion inhibition efficiency analysis (Figures 4 and 5).
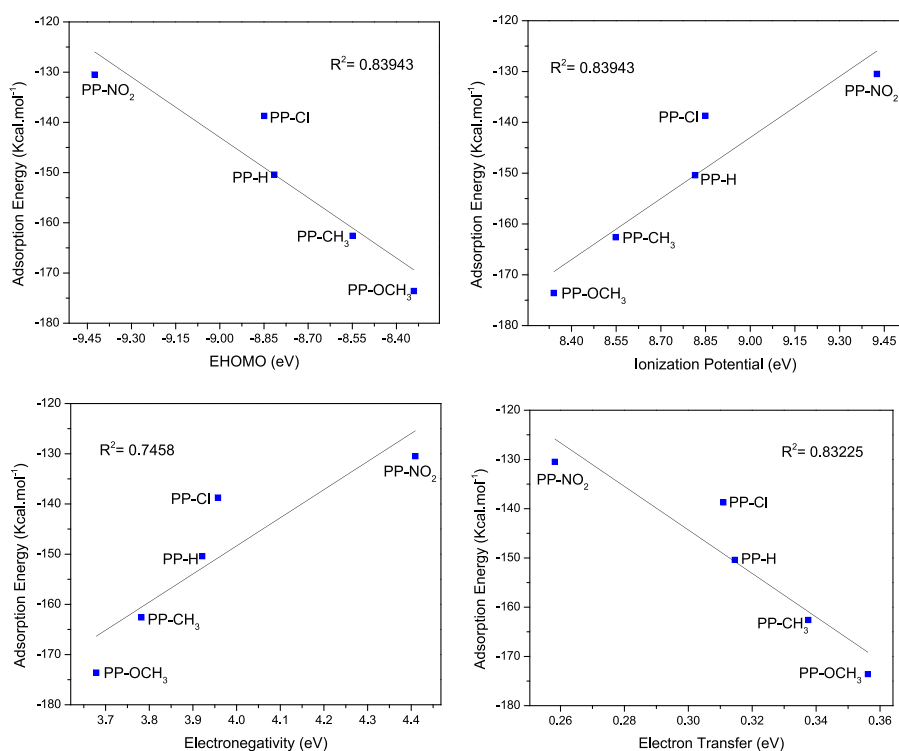
Figure 7. Phenyl phthalimide and its derivatives under neutral inhibitor conditions: correlation of adsorption energy and quantum chemical parameters.
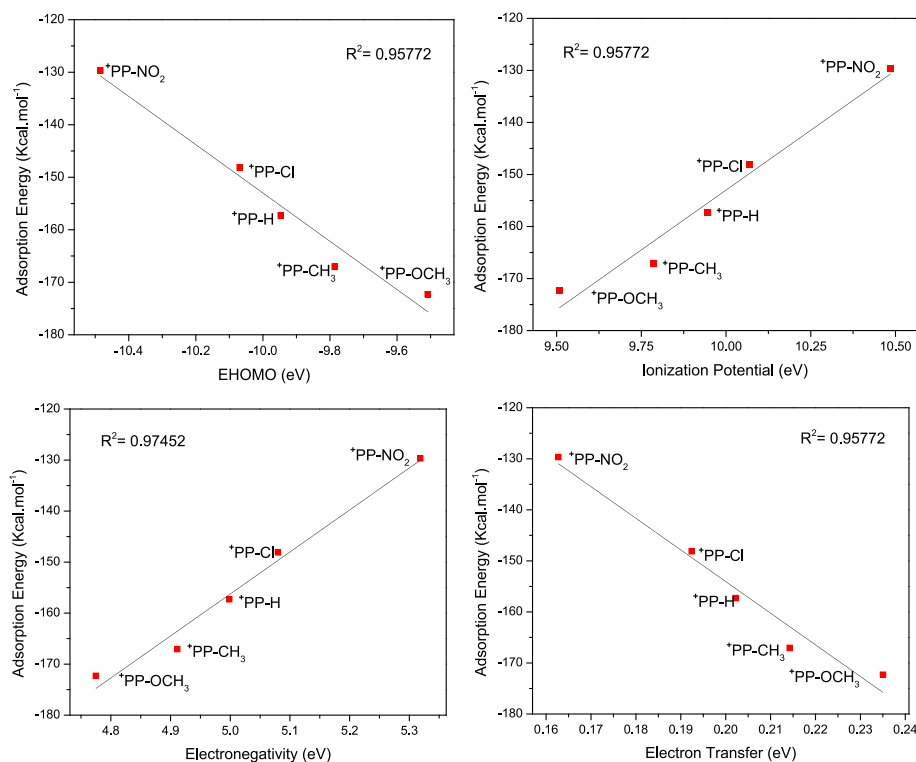
Figure 8. Phenyl phthalimide and its derivatives under protonated inhibitor conditions: correlation of adsorption energy and quantum chemical parameters.

The adsorption of organic corrosion inhibitors on the carbon steel metal surface occurs through donor−acceptor interactions, which can be analyzed by local reactivity, namely, the Fukui function. Fukui's function measures chemical reactivity and shows the nucleophilic and electrophilic attack of organic inhibitors. Nucleophilic and electrophilic attacks can occur in the presence of maximum f^+ and f^- values.[63−65] The greater the value of the Fukui function, the more reactive the active site of a molecule.

The f_K^+ value indicates the preferable sites for nucleophilic attack or when the molecule receives electrons, whereas the f_K^- value indicates the preferable sites for electrophilic attack or when the molecule donates electrons.[66,67] Equations 6 and 7 can be used to calculate the Fukui function's value. Table 6 shows that the most reactive sites of PP-H and PP-CH$_3$ for nucleophilic attack are in N8 and C13 atoms, PP-OCH$_3$ in N8, C14, and O26 atoms, respectively, PP-Cl on N8 and Cl18 atoms, and PP-NO$_2$ in N8 and C15 atoms. The atom shows that it is most likely to accept electrons from the surface of Fe(110), thus forming a back bond. The maximum f_K^- values of PP-H, PP-CH$_3$, and PP-OCH$_3$ for electrophilic attack are located in O16 and O17 atoms. PP-Cl and PP-NO$_2$ are located at C3 and C6 atoms and O19 and O20 atoms, respectively. This demonstrated a propensity for donating electrons to an open d orbital on the surface of Fe(110) in order to create a coordinate bond.

Monte Carlo simulations can be used to demonstrate the mechanism of corrosion inhibition by organic inhibitors on metal surfaces. The Monte Carlo simulation tries to find the lowest energy for all systems.[68,69] Monte Carlo simulations were carried out on inhibitors (PP-H, PP-CH$_3$, PP-OCH$_3$, PP-Cl, and PP-NO$_2$), 100 water molecules, and a carbon steel surface represented by Fe(110). Figure 6 shows the Monte Carlo simulation of the most stable adsorption conformation of each organic inhibitor (PP-H, PP-CH$_3$, PP-OCH$_3$, PP-Cl, and PP-NO$_2$) on the surface of Fe(110) and 100 water molecules. The distance between the atoms in the organic inhibitor and the metal surface can help understand the adsorption process's nature. A distance value less than 3.5 indicates chemical adsorption (chemisorption), while a distance value greater than 3.5 indicates physical adsorption (physisorption).[70,71] A higher negative adsorption energy value indicates a more stable and stronger interaction between organic inhibitors of carbon steel.[72,73] Table 7 shows that the highest adsorption energy value for the organic inhibitor PP-OCH$_3$ was obtained at -173.5912 kcal mol^{-1}. The order of adsorption energy is PP-OCH$_3$ > PP-CH$_3$ > PP-H > PP-Cl > PP-NO2. This sequence is the same result of MP2/6-311++G (d,p) quantum chemistry calculations in the solution phase. Table 7 shows that the adsorption energies of the corrosion inhibitors are higher than the adsorption energies of the water molecules. This demonstrates how water molecules can be gradually replaced by inhibitor molecules on the carbon steel surface, forming a stable layer that protects the carbon steel from aqueous corrosion. The experimental results of the previously reported corrosion inhibition efficiency are linearly correlated with the Monte Carlo simulation studies that have been carried out. PP and its derivatives have a lone pair of electrons, such as nitrogen and oxygen atoms, so it is possible to donate electrons to the empty d orbital on the Fe(110) surface to form a stable coordination bond. Therefore, PP and its derivatives can cover and form a protective layer of carbon steel from corrosive substances in the solution. A short bond distance <3.5 Å between the inhibitor and metal often indicates chemisorption, while a higher bond length >3.5 Å suggests physisorption. The average bond length of all inhibitors was Fe−O 2.850−2.980 Å, Fe−N 2.900−2.998 Å, and Fe−C 2.970−3.00 Å. This indicates the occurrence of chemical interactions between N, O, and C-benzene atoms and the Fe(110) surface. Figures 7 and 8 show a linear correlation between the adsorption energy and quantum chemical parameters of phenyl phthalimide and its derivatives under neutral circumstances. Adsorption is widely accepted as the primary mechanism of corrosion inhibitors interacting with carbon steel. As a result, the adsorption energy can be used to rank inhibitory molecules directly. The most stable and strong adsorption system has high negative adsorption energy.[74,75]

4. CONCLUSIONS

Theoretical studies have been carried out to elucidate the corrosion inhibitory mechanism of phenyl phthalimide and its derivatives as corrosion inhibitors against carbon steels. DFT and ab initio MP2 explain quantum parameters' influence on corrosion inhibition efficiency. In addition, the reactive site of the inhibitor, which contributes maximally to the corrosion inhibition process, has also been described. Fukui function analysis showed that nitrogen, oxygen, and phenyl carbon atoms became the main reactive sites of corrosion inhibitors; the reactive site can donate electrons to the carbon steel surface. The Monte Carlo simulation can also provide an overview of the mechanism between the organic inhibitor, 100 water molecules, and the carbon steel surface. The highest negative adsorption energy was obtained from the organic inhibitor PP-OCH$_3$ of -173.5912 kcal mol^{-1}. In an aqueous solution, all the organic inhibitors studied were able to compete with water so that they could be adsorbed on the metal surface. PP-OCH$_3$ contributes very well to inhibiting corrosion of carbon steel. The result follows the corrosion inhibition efficiency test conducted previously. This theoretical study can be a bridge in solving problems related to the electronic properties of corrosion inhibitors.

■ AUTHOR INFORMATION

Corresponding Author

Saprizal Hadisaputra − *Chemistry Education Division, University of Mataram, Mataram 83125, Indonesia;* ⓞ orcid.org/0000-0002-0386-4571; Email: rizal@unram.ac.id

Authors

Agus Abhi Purwoko − *Chemistry Education Division, University of Mataram, Mataram 83125, Indonesia*

Aliefman Hakim − *Chemistry Education Division, University of Mataram, Mataram 83125, Indonesia*

Niko Prasetyo − *Austrian-Indonesian Centre for Computational Chemistry, Universitas Gadjah Mada, Sekip Utara, Yogyakarta 55281, Indonesia*

Saprini Hamdiani − *Department of Applied Chemistry, Chaoyang University of Technology, Taichung 41349, Taiwan*

Complete contact information is available at:
https://pubs.acs.org/10.1021/acsomega.2c03091

Notes

The authors declare no competing financial interest.

■ REFERENCES

(1) Dwivedi, D.; Lepková, K.; Becker, T. Carbon steel corrosion: a review of key surface properties and characterization methods. *RSC Adv.* **2017**, *7*, 4580−4610.

(2) Kobzar, Y. L.; Fatyeyeva, K. Ionic liquids as green and sustainable steel corrosion inhibitors: Recent developments. *Chem. Eng. J.* **2021**, *425*, 131480.

(3) Asmara, Y. P.; Kurniawan, T. Corrosion prediction for corrosion rate of carbon steel in oil and gas environment: A review. *Indones. J. Sci. Technol.* **2018**, *3*, 64−74.

(4) Finšgar, M.; Jackson, J. Application of corrosion inhibitors for steels in acidic media for the oil and gas industry: A review. *Corros. Sci.* **2014**, *86*, 17−41.

(5) Refait, P.; Grolleau, A. M.; Jeannin, M.; Rémazeilles, C.; Sabot, R. Corrosion of carbon steel in marine environments: role of the corrosion product layer. *Corros. Mater. Degrad.* **2020**, *1*, 198−218.

(6) Monteiro, G. P.; Tavares, I. M. D. C.; de Carvalho, M. C. F.; Carvalho, M. S.; Pimentel, A. B.; Santos, P. H.; Franco, M. Evaluation of fungal biomass developed from cocoa by-product as a substrate with corrosion inhibitor for carbon steel. *Chem. Eng. Commun.* **2022**, 1−16.

(7) Hsissou, R.; Abbout, S.; Seghiri, R.; Rehioui, M.; Berisha, A.; Erramli, H.; Elharfi, A. Evaluation of corrosion inhibition performance of phosphorus polymer for carbon steel in [1 M] HCl: Computational studies (DFT, MC and MD simulations). *J. Mater. Res. Technol.* **2020**, *9*, 2691−2703.

(8) Cherrad, S.; Alrashdi, A. A.; Lee, H. S.; Lgaz, H.; Satrani, B.; Ghanmi, M.; Chaouch, A. Cupressus arizonica fruit essential oil: A novel green inhibitor for acid corrosion of carbon steel. *Arab. J. Chem.* **2022**, *15*, 103849.

(9) Al Kiey, S. A.; Hasanin, M. S.; Dacrory, S. Potential anticorrosive performance of green and sustainable inhibitor based on cellulose derivatives for carbon steel. *J. Mol. Liq.* **2021**, *338*, 116604.

(10) Murmu, M., Saha, S. K., Murmu, N. C., Banerjee, P. Corrosion Inhibitors for Acidic Environments. In *Sustainable Corrosion Inhibitors I: Fundamentals, Methodologies, and Industrial Applications*; American Chemical Society, (2021). *1403* (111−162).

(11) Chauhan, D. S.; Verma, C.; Quraishi, M. A. Molecular structural aspects of organic corrosion inhibitors: Experimental and computational insights. *J. Mol. Struct.* **2021**, *1227*, 129374.

(12) Quraishi, M. A.; Chauhan, D. S.; Ansari, F. A. Development of environmentally benign corrosion inhibitors for organic acid environments for oil-gas industry. *J. Mol. Liq.* **2021**, *329*, 115514.

(13) Qiang, Y.; Guo, L.; Li, H.; Lan, X. Fabrication of environmentally friendly Losartan potassium film for corrosion inhibition of mild steel in HCl medium. *Chem. Eng. J.* **2021**, *406*, 126863.

(14) Quraishi, M. A.; Chauhan, D. S.; Saji, V. S. Heterocyclic biomolecules as green corrosion inhibitors. *J. Mol. Liq.* **2021**, *341*, 117265.

(15) Hossain, N.; Asaduzzaman Chowdhury, M.; Kchaou, M. An overview of green corrosion inhibitors for sustainable and environment friendly industrial development. *J. Adhes. Sci. Technol.* **2021**, *35*, 673−690.

(16) Verma, C., Quraishi, M. A., Ebenso, E. E., Hussain, C. M. Amines as Corrosion Inhibitors: A Review. *Organic Corrosion Inhibitors: Synthesis, Characterization, Mechanism, and Applications*; John Wiley & Sons, Inc., (2021), 75−94.

(17) Zaafarany, I. Phenyl phthalimide as corrosion inhibitor for corrosion of C-Steel in sulphuric acid solution. *Port. Electrochim. Acta* **2009**, *27*, 631−643.

(18) Donkor, S.; Song, Z.; Jiang, L.; Chu, H. An overview of computational and theoretical studies on analyzing adsorption performance of phytochemicals as metal corrosion inhibitors. *J. Mol. Liq.* **2022**, *359*, 119260.

(19) Pham, T. L. M.; Phung, T. K.; Thang, H. V. DFT insights into the adsorption mechanism of five-membered aromatic heterocycles containing N, O, or S on Fe (110) surface. *Appl. Surf. Sci.* **2022**, *583*, 152524.

(20) Ebenso, E. E.; Verma, C.; Olasunkanmi, L. O.; Akpan, E. D.; Verma, D. K.; Lgaz, H.; Quraishi, M. A. Molecular modelling of compounds used for corrosion inhibition studies: a review. *Phys. Chem. Chem. Phys.* **2021**, *23*, 19987−20027.

(21) Verma, D. K.; Aslam, R.; Aslam, J.; Quraishi, M. A.; Ebenso, E. E.; Verma, C. Computational modeling: theoretical predictive tools for designing of potential organic corrosion inhibitors. *J. Mol. Struct.* **2021**, *1236*, 130294.

(22) Hadisaputra, S.; Purwoko, A. A.; Wajdi, F.; Sumarlan, I.; Hamdiani, S. Theoretical study of the substituent effect on corrosion inhibition performance of benzimidazole and its derivatives. *Int. J. Corros. Scale Inhib.* **2019**, *8*, 673−688.

(23) Chiter, F.; Costa, D.; Maurice, V.; Marcus, P. DFT investigation of 2-mercaptobenzothiazole adsorption on model oxidized copper surfaces and relationship with corrosion inhibition. *Appl. Surf. Sci.* **2021**, *537*, 147802.

(24) Berisha, A. Ab inito exploration of nanocars as potential corrosion inhibitors. *Comput. Theor. Chem.* **2021**, *1201*, 113258.

(25) Lgaz, H.; Lee, H. S. Ab-initio DFT Modeling of Alkanethiols as Carbon Steel Corrosion Inhibitors. In *Proceedings of the Korean Institute of Building Construction Conference*; The Korean Institute of Building Construction. 2021 (91−92).

(26) Haris, N. I. N.; Sobri, S.; Yusof, Y. A.; Kassim, N. K. An overview of molecular dynamic simulation for corrosion inhibition of ferrous metals. *Metals* **2021**, *11*, 46.

(27) Dahmani, K.; Galai, M.; Ouakki, M.; Cherkaoui, M.; Touir, R.; Erkan, S.; Kaya, S.; El Ibrahimi, B. Quantum chemical and molecular dynamic simulation studies for the identification of the extracted cinnamon essential oil constituent responsible for copper corrosion inhibition in acidified 3.0 wt% NaCl medium. *Inorg. Chem. Commun.* **2021**, *124*, 108409.

(28) Sulaiman, K. O.; Onawole, A. T.; Faye, O.; Shuaib, D. T. Understanding the corrosion inhibition of mild steel by selected green compounds using chemical quantum based assessments and molecular dynamics simulations. *J. Mol. Liq.* **2019**, *279*, 342−350.

(29) Hadisaputra, S.; Purwoko, A. A.; Savalas, L. R. T.; Prasetyo, N.; Yuanita, E.; Hamdiani, S. Quantum chemical and Monte Carlo simulation studies on inhibition performance of caffeine and its derivatives against corrosion of copper. *Coatings* **2020**, *10*, 1086.

(30) Hadisaputra, S.; Purwoko, A. A.; Hamdiani, S. Copper Corrosion Protection by 4-Hydrocoumarin Derivatives: Insight from Density Functional Theory, Ab Initio, and Monte Carlo Simulation Studies. *Indones. J. Chem.* **2021**, *22*, 413−428.

(31) Abdulazeez, I.; Khaled, M.; Al-Saadi, A. A. Impact of electron-withdrawing and electron-donating substituents on the corrosion inhibitive properties of benzimidazole derivatives: a quantum chemical study. *J. Mol. Struct.* **2019**, *1196*, 348−355.

(32) Assad, H.; Kumar, A. Understanding functional group effect on corrosion inhibition efficiency of selected organic compounds. *J. Mol. Liq.* **2021**, *344*, 117755.

(33) Hadisaputra, S.; Purwoko, A. A.; Hamdiani, S. Substituents effects on the corrosion inhibition performance of pyrazolone against carbon steels: quantum chemical and Monte Carlo simulation studies. *Int. J. Corros. Scale Inhib.* **2021**, *10*, 419−440.

(34) Shamov, G. A.; Schreckenbach, G.; Martin, R. L.; Hay, P. J. Crown ether inclusion complexes of the early actinide elements, [AnO2 (18-crown-6)] n+, An= U, Np, Pu and n= 1, 2: A relativistic density functional study. *Inorg. Chem.* **2008**, *47*, 1465−1475.

(35) Fan, Y.; Li, Y.; Shu, X.; Wu, R.; Chen, S.; Jin, Y.; Xia, C. Complexation and Separation of Trivalent Actinides and Lanthanides by a Novel DGA Derived from Macrocyclic Crown Ether: Synthesis, Extraction, and Spectroscopic and Density Functional Theory Studies. *ACS Omega* **2021**, *6*, 2156−2166.

(36) Hadisaputra, S.; Canaval, L. R.; Pranowo, H. D.; Armunanto, R. Theoretical study of substituent effects on Cs+/Sr2+−dibenzo-18-crown-6 complexes. *Monatsh. Chem.* **2014**, *145*, 737−745.

(37) Frisch, M.J.; Trucks, G.W.; Schlegel, H.B.; Scuseria, G.E., Robb, M.A., Cheeseman, J.R.; Scalmani, G.; Barone, V.; Petersson, G. A.; Nakatsuji, H.; Li, X.; Caricato, M.; Marenich, A. V.; Bloino, J.; Janesko, B. G.; Gomperts, R.; Mennucci, B.; Hratchian, H. P.; Ortiz, J. V.; Izmaylov, A. F.; Sonnenberg, J. L.; Williams-Young, D.; Ding, F.; Lipparini, F.; Egidi, F.; Goings, J.; Peng, B.; Petrone, A.; Henderson, T.; Ranasinghe, D.; Zakrzewski, V. G.; Gao, J.; Rega, N.; Zheng, G.;

Liang, W.; Hada, M.; Ehara, M.; Toyota, K.; Fukuda, R.; Hasegawa, J.; Ishida, M.; Nakajima, T.; Honda, Y.; Kitao, O.; Nakai, H.; Vreven, T.; Throssell, K.; Montgomery, J. A., Jr.; Peralta, J. E.; Ogliaro, F.; Bearpark, M. J.; Heyd, J. J.; Brothers, E. N.; Kudin, K. N.; Staroverov, V. N.; Keith, T. A.; Kobayashi, R.; Normand, J.; Raghavachari, K.; Rendell, A. P.; Burant, J. C.; Iyengar, S. S.; Tomasi, J.; Cossi, M.; Millam, J. M.; Klene, M.; Adamo, C.; Cammi, R.; Ochterski, J. W.; Martin, R. L.; Morokuma, K.; Farkas, O.; Foresman, J. B.; Fox, D. J., *4. Gaussian09, R*; Gaussian. Inc.: Wallingford. (2009). 02.

(38) Koopmans, T. Über die Zuordnung von Wellenfunktionen und Eigenwerten zu den einzelnen Elektronen eines Atoms. *Physica* **1934**, *1*, 104−113.

(39) Pearson, R. G. Absolute electronegativity and hardness: application to inorganic chemistry. *Inorg. Chem.* **1988**, 27, 734−740.

(40) Pearson, R. G. Hard and soft acids and bases—the evolution of a chemical concept. *Coord. Chem. Rev.* **1990**, *100*, 403−425.

(41) Martinez, S. Inhibitory mechanism of mimosa tannin using molecular modeling and substitutional adsorption isotherms. *Mater. Chem. Phys.* **2003**, *77*, 97−102.

(42) Erdoğan, Ş.; Safi, Z. S.; Kaya, S.; Işın, D. Ö.; Guo, L.; Kaya, C. A computational study on corrosion inhibition performances of novel quinoline derivatives against the corrosion of iron. *J. Mol. Struct.* **2017**, *1134*, 751−761.

(43) Islam, N.; Chandra Ghosh, D. A new algorithm for the evaluation of the global hardness of polyatomic molecules. *Mol. Phys.* **2011**, *109*, 917−931.

(44) Frenkel, D.; Smit, B. *Understanding Molecular Simulations: from Algorithms to Applications*, 2nd ed.; Academic Press: San Diego, 2002.

(45) Kirkpatrick, S.; Gelatt, C. D.; Vecchi, M. P. Optimization by simulated annealing. *Science* **1983**, *220*, 671−680.

(46) Alahiane, M.; Oukhrib, R.; Albrimi, Y. A.; Abou Oualid, H.; Bourzi, H.; Akbour, R. A.; et al. Experimental and theoretical investigations of benzoic acid derivatives as corrosion inhibitors for AISI 316 stainless steel in hydrochloric acid medium: DFT and Monte Carlo simulations on the Fe (110) surface. *RSC Adv.* **2020**, *10*, 41137−41153.

(47) Guo, L.; Qi, C.; Zheng, X.; Zhang, R.; Shen, X.; Kaya, S. Toward understanding the adsorption mechanism of large size organic corrosion inhibitors on an Fe (110) surface using the DFTB method. *RSC Adv.* **2017**, *7*, 29042−29050.

(48) Kaya, S.; Tüzün, B.; Kaya, C.; Obot, I. B. Determination of corrosion inhibition effects of amino acids: quantum chemical and molecular dynamic simulation study. *J. Taiwan Inst. Chem. Eng.* **2016**, *58*, 528−535.

(49) Madkour, L. H.; Kaya, S.; Guo, L.; Kaya, C. Quantum chemical calculations, molecular dynamic (MD) simulations and experimental studies of using some azo dyes as corrosion inhibitors for iron. Part 2: Bis−azo dye derivatives. *J. Mol. Struct.* **2018**, *1163*, 397−417.

(50) Tanak, H.; Yakan, H.; Kütük, H.; Karakullukçu, N. T.; Dege, N. Crystal and Molecular Structure of N-(Phenylthio) phthalimide. *Crystallogr. Rep.* **2018**, *63*, 379−381.

(51) Alaoui, K.; Ouakki, M.; Abousalem, A. S.; Serrar, H.; Galai, M.; Derbali, S.; El Kacimi, Y. Molecular dynamics, Monte-Carlo simulations and atomic force microscopy to study the interfacial adsorption behaviour of some triazepine carboxylate compounds as corrosion inhibitors in acid medium. *J. Bio Tribo-Corros.* **2019**, *5*, 1−16.

(52) Oyeneyin, O. E.; Ojo, N. D.; Ipinloju, N.; James, A. C.; Agbaffa, E. B. Investigation of Corrosion Inhibition Potentials of Some Aminopyridine Schiff Bases Using Density Functional Theory and Monte Carlo Simulation. *Chemistry Africa* **2022**, *5*, 319−332.

(53) Hadisaputra, S.; Purwoko, A. A.; Rahmawati, R.; Asnawati, D.; Ilhamsyah, I.; Hamdiani, S.; Nuryono, N. Experimental and Theoretical Studies of (2R)-5-hydroxy-7methoxy-2-phenyl-2, 3-dihydrochromen-4-one as corrosion inhibitor for Iron in Hydrochloric Acid. *Int. J. Electrochem. Sci.* **2019**, *14*, 11110−11121.

(54) Zohdy, K. M.; El-Shamy, A. M.; Kalmouch, A.; Gad, E. A. The corrosion inhibition of (2Z, 2′ Z)-4, 4′-(1, 2-phenylene bis (azanediyl)) bis (4-oxobut-2-enoic acid) for carbon steel in acidic media using DFT. *Egypt. J. Pet.* **2019**, *28*, 355−359.

(55) Guo, L.; Safi, Z. S.; Kaya, S.; Shi, W.; Tüzün, B.; Altunay, N.; Kaya, C. Anticorrosive effects of some thiophene derivatives against the corrosion of iron: a computational study. *Front. Chem.* **2018**, *6*, 155.

(56) Jamil, D. M.; Al-Okbi, A. K.; Al-Baghdadi, S. B.; Al-Amiery, A. A.; Kadhim, A.; Gaaz, T. S.; Mohamad, A. B. Experimental and theoretical studies of Schiff bases as corrosion inhibitors. *Chem. Cent. J.* **2018**, *12*, 7.

(57) Kokalj, A. On the alleged importance of the molecular electron-donating ability and the HOMO−LUMO gap in corrosion inhibition studies. *Corros. Sci.* **2021**, *180*, 109016.

(58) Reimers, J. R.; CAI, Z. L.; Bilić, A.; Hush, N. S. The Appropriateness of Density-Functional Theory for the Calculation of Molecular Electronics Properties. *Ann. N. Y. Acad. Sci.* **2003**, *1006*, 235−251.

(59) Cotter, J. L.; Dine-Hart, R. A. Ionization and dissociation of some aromatic imides under electron impact. *Chem. Commun.* **1966**, *22*, 809−810.

(60) Parr, R. G.; Szentpály, L. V.; Liu, S. Electrophilicity index. *J. Am. Chem. Soc.* **1999**, *121*, 1922−1924.

(61) Chattaraj, P. K.; Giri, S. Electrophilicity index within a conceptual DFT framework. *Annu. Rep. Prog. Chem., Sect. C: Phys. Chem.* **2009**, *105*, 13−39.

(62) Lukovits, I.; Kalman, E.; Zucchi, F. Corrosion inhibitors—correlation between electronic structure and efficiency. *Corrosion* **2001**, *57*, 3−8.

(63) Fuentealba, P.; Pérez, P.; Contreras, R. On the condensed Fukui function. *J. Chem. Phys.* **2000**, *113*, 2544−2551.

(64) Yang, W.; Parr, R. G. Hardness, softness, and the fukui function in the electronic theory of metals and catalysis. *Proc. Natl. Acad. Sci. U. S. A.* **1985**, *82*, 6723−6726.

(65) Wang, H.; Wang, X.; Wang, H.; Wang, L.; Liu, A. DFT study of new bipyrazole derivatives and their potential activity as corrosion inhibitors. *J. Mol. Model.* **2006**, *13*, 147−153.

(66) Wazzan, N. A.; Obot, I. B.; Kaya, S. Theoretical modeling and molecular level insights into the corrosion inhibition activity of 2-amino-1, 3, 4-thiadiazole and its 5-alkyl derivatives. *J. Mol. Liq.* **2016**, *221*, 579−602.

(67) Dehghani, A.; Bahlakeh, G.; Ramezanzadeh, B.; Mostafatabar, A. H. Construction of a zinc-centered metal−organic film with high anti-corrosion potency through covalent-bonding between the natural flavonoid-based molecules (Quercetin)/divalent-zinc: Computer modeling (integrated-DFT&MC/MD)/electrochemical-surface assessments. *J. Ind. Eng. Chem.* **2020**, *88*, 382−395.

(68) El Ibrahimi, B.; Jmiai, A.; El Mouaden, K.; Oukhrib, R.; Soumoue, A.; El Issami, S.; Bazzi, L. Theoretical evaluation of some α-amino acids for corrosion inhibition of copper in acidic medium: DFT calculations, Monte Carlo simulations and QSPR studies. *J. King Saud Univ. Sci.* **2020**, *32*, 163−171.

(69) Mashuga, M. E.; Olasunkanmi, L. O.; Lgaz, H.; Sherif, E. S. M.; Ebenso, E. E. Aminomethylpyridazine isomers as corrosion inhibitors for mild steel in 1 M HCl: Electrochemical, DFT and Monte Carlo simulation studies. *J. Mol. Liq.* **2021**, *344*, 117882.

(70) Hsissou, R.; Benhiba, F.; Dagdag, O.; El Bouchti, M.; Nouneh, K.; Assouag, M.; Elharfi, A. Development and potential performance of prepolymer in corrosion inhibition for carbon steel in 1.0 M HCl: outlooks from experimental and computational investigations. *J. Colloid Interface Sci.* **2020**, *574*, 43−60.

(71) Sastri, V. S.; Elboujdaini, M.; Perumareddi, J. R. Utility of quantum chemical parameters in the rationalization of corrosion inhibition efficiency of some organic inhibitors. *Corrosion* **2005**, *61*, 933−942.

(72) El-Hajjaji, F.; Belghiti, M. E.; Hammouti, B.; Jodeh, S.; Hamed, O.; Lgaz, H.; Salghi, R. Adsorption and corrosion inhibition effect of 2-mercaptobenzimidazole (surfactant) on a carbon steel surface in an acidic medium: Experimental and monte carlo simulations. *Port. Electrochim. Acta* **2018**, *36*, 197−212.

(73) Dehdab, M.; Yavari, Z.; Darijani, M.; Bargahi, A. The inhibition of carbon-steel corrosion in seawater by streptomycin and tetracycline antibiotics: an experimental and theoretical study. *Desalination* **2016**, *400*, 7−17.

(74) Kumar, D.; Jain, N.; Jain, V.; Rai, B. Amino acids as copper corrosion inhibitors: A density functional theory approach. *Appl. Surf. Sci.* **2020**, *514*, 145905.

(75) Obot, I. B.; Kaya, S.; Kaya, C.; Tüzün, B. Density Functional Theory (DFT) modeling and Monte Carlo simulation assessment of inhibition performance of some carbohydrazide Schiff bases for steel corrosion. *Phys. E Low Dimens. Syst. Nanostruct.* **2016**, *80*, 82−90.